

Secular behavior of electrostatic Kelvin–Helmholtz (diocotron) modes coupled with plasma oscillations

M. Hirota, T. Tatsuno, S. Kondoh, and Z. Yoshida

Graduate School of Frontier Sciences, The University of Tokyo, Tokyo 113-0033, Japan

(Received 21 June 2001; accepted 18 December 2001)

Electrostatic instabilities in electron plasmas have been studied by analyzing initial value problems. The self-electric field of a non-neutral plasma produces a flow that brings about non-Hermitian property into the generating operator. Because of the nonorthogonality of eigenmodes, the evolution of the system is rather complex. Secular behavior is a typical appearance of unresolvable mode couplings that may be cast in a representation of Jordan block. The coupling of the perpendicular (with respect to the magnetic field) electrostatic modes (Kelvin–Helmholtz or diocotron modes) and parallel plasma oscillations causes a more complex phenomena. © 2002 American Institute of Physics. [DOI: 10.1063/1.1454123]

I. INTRODUCTION

Because of the increasing interest in many effects of sheared plasma flows, the Kelvin–Helmholtz instabilities and related phenomena are receiving careful reconsideration. A non-neutral plasma, supporting an unbalanced internal electric field, self-generates an intense flow that may have strong shear.^{1–3} It provides paradigms of general vortical dynamics, which encompass various plasma phenomena, galactic dynamics, atmospheric fluid mechanics, and so on.

References 4 and 5 have considered the most general relativistic electromagnetic perturbations propagating perpendicular to the magnetic field, including both the polarization drift ($\propto \partial \mathbf{E} / \partial t$) and the $\mathbf{E} \times \mathbf{B}$ drift in the dielectric response function. The polarization susceptibility, which is proportional to ω_p^2 / ω_c^2 (with ω_p = plasma frequency and ω_c = cyclotron frequency) leads to an essential singularity in the eigenmode equation, causing the existence of a continuous spectrum. Another mode continuum, which however was neglected in Refs. 4 and 5, is now introduced in the present work. This continuum, originating from the flow shear, persists in the low space charge limit $\omega_p^2 / \omega_c^2 \rightarrow 0$ (i.e., neglecting the polarization drift), and plays an important role in producing non-Hermiticity. The present work considers oblique propagation, coupling the transverse mode with electrostatic modes parallel to the magnetic field. The presence of the continuum significantly changes the time evolution of the diocotron modes.

In the low density limit ($\omega_p / \omega_c \ll 1$), the flow in a non-neutral plasma equilibrium is approximated by the $\mathbf{E} \times \mathbf{B}$ drift velocity. When \mathbf{B} is homogeneous, the electrostatic potential ϕ obeys the standard vortex equation in the plane perpendicular with respect to \mathbf{B} . Comparing ϕ with the stream function of a two-dimensional incompressible flow, the electrostatic modes (so-called diocotron modes) parallels the Kelvin–Helmholtz modes in a shear flow.^{6–9}

The aim of this paper is to analyze rather complex phenomena induced by a coupling of the Kelvin–Helmholtz modes with parallel (with respect to \mathbf{B}) plasma oscillations, which becomes important when we consider a sheared mag-

netic field.¹⁰ This complexity is primarily due to the non-Hermitian property of the Kelvin–Helmholtz modes. The interaction of fluctuations and the ambient shear flow cannot be cast in a Hamiltonian form, and hence, the generator of the dynamics must be a non-Hermitian operator.^{11–13} A general non-Hermitian operator does not have a complete set of orthogonal eigenfunctions. When eigenfunctions are not complete to span the whole function space, one has to consider the nilpotent which brings about secular behavior of type $t^n e^{i\omega t}$. The amplitude of perturbation can increase algebraically even if every eigenvalue ω is real. In a finite dimensional linear space, a non-Hermitian map can be written as a Jordan matrix. However, we do not have a spectral representation theory for a general non-Hermitian operator in an infinite dimensional Hilbert space.

In this paper, we demonstrate secular behavior of Kelvin–Helmholtz modes by solving initial value problems numerically. We formulate a one dimensional model in an integral equation form, and use the trapezoidal rule for numerical integration. Analyzing the structure of the generator, we show that the secular behavior is caused by internal resonances of the perpendicular (with respect to the magnetic field) electrostatic modes and parallel plasma oscillations.

II. FORMULATION

We consider an electron plasma in a slab geometry of finite thickness. An external magnetic field (\mathbf{B}) is applied to confine the plasma. The $\mathbf{E} \times \mathbf{B}$ drift is induced by the self-electric field (\mathbf{E}), which may create a flow shear. When the electron density is sufficiently small, we may ignore the magnetic perturbations induced by the internal current.

The system is governed by

$$\frac{\partial n}{\partial t} + \nabla \cdot (n \mathbf{v}) = 0, \quad (1)$$

$$\frac{\partial \mathbf{v}}{\partial t} + (\mathbf{v} \cdot \nabla) \mathbf{v} = -\frac{e}{m} (-\nabla \phi + \mathbf{v} \times \mathbf{B}), \quad (2)$$

$$\nabla^2 \phi = \frac{e}{\epsilon_0} n, \quad (3)$$

where n is the electron number density, \mathbf{v} is the plasma velocity, e is the elementary charge, m is the electron mass, and ϕ is the electrostatic potential ($\mathbf{E} = -\nabla\phi$). We have neglected the thermal pressure of electrons. The ambient magnetic field is, in Cartesian coordinates,

$$\mathbf{B}(x) = (0, B_y(x), B_z), \quad (4)$$

where B_z is a constant (this \mathbf{B} is not curl-free, but it does not cause essential difficulty in the present theory). We consider a simple equilibrium with a flat top density,

$$n = N(x) = \begin{cases} \bar{N} & (|x| \leq L), \\ 0 & (|x| > L), \end{cases} \quad (5)$$

where $2L$ corresponds to the thickness of slab plasma. The equilibrium flow velocity is given by (2);

$$\mathbf{v} = \mathbf{V}(x) = \frac{-\nabla\Phi(x) \times \mathbf{B}(x)}{B(x)^2}, \quad (6)$$

where $B(x) = \sqrt{B_y^2(x) + B_z^2}$, and $\nabla\Phi(x) = (e\bar{N}x/\epsilon_0, 0, 0)$ for $|x| \leq L$.

We normalize the variables as

$$\hat{n} = \frac{n}{\bar{N}}, \quad \hat{t} = 2\omega_D t, \quad \hat{\mathbf{r}} = \frac{\mathbf{r}}{L} [\mathbf{r} = (x, y, z)], \quad (7)$$

$$\hat{\mathbf{v}} = \frac{\mathbf{v}}{\bar{V}}, \quad \hat{\mathbf{B}} = \frac{\mathbf{B}}{B_z}, \quad \hat{\mathbf{E}} = \frac{\mathbf{E}}{\bar{E}},$$

where

$$\omega_D \equiv \frac{e\bar{N}}{2\epsilon_0 B_z}, \quad (8)$$

$$\bar{V} \equiv 2L\omega_D, \quad (9)$$

$$\bar{E} \equiv \bar{V}B_z. \quad (10)$$

The $\omega_D (= \omega_p^2/2\omega_c)$ is called ‘‘diocotron frequency.’’ In what follows, we omit the $\hat{}$ to simplify notation.

We decompose unknown variables (n, ϕ, \mathbf{v}) into equilibrium quantities (capital letters) and perturbations (tildes). Linearizing (1)–(3) for perturbations, we obtain

$$\frac{\partial \tilde{n}}{\partial t} + \mathbf{V} \cdot \nabla \tilde{n} + \nabla \cdot (N \tilde{\mathbf{v}}_{\perp}) + \nabla \cdot (N \tilde{\mathbf{v}}_{\parallel}) = 0, \quad (11)$$

$$\frac{\partial \tilde{\mathbf{v}}_{\parallel}}{\partial t} + (\mathbf{V} \cdot \nabla) \tilde{\mathbf{v}}_{\parallel} = \frac{1}{s^2} \nabla_{\parallel} \tilde{\phi}, \quad (12)$$

$$\nabla^2 \tilde{\phi} = \tilde{n}, \quad (13)$$

where $s \equiv \omega_p/\omega_c$ is a dimensionless scaling parameter. Here we assume $s \ll 1$ (low density). In the above equations, $\tilde{\mathbf{v}}_{\parallel}$ and $\tilde{\mathbf{v}}_{\perp}$, respectively, denote the parallel and perpendicular

components of $\tilde{\mathbf{v}}$ with respect to the ambient magnetic field. Assuming low density, we may appeal to the guiding-center approximation⁴

$$\tilde{\mathbf{v}}_{\perp} = \frac{-\nabla \tilde{\phi} \times \mathbf{B}}{B^2}. \quad (14)$$

We Fourier transform the perturbations with respect to y and z , and denote the corresponding wave numbers by k_y and k_z . We introduce sheared coordinates defined by

$$\eta(x) = \frac{B_z}{B(x)} y - \frac{B_y(x)}{B(x)} z, \quad (15)$$

$$\zeta(x) = \frac{B_y(x)}{B(x)} y + \frac{B_z}{B(x)} z. \quad (16)$$

The corresponding wave numbers are given by

$$k_{\perp}(x) = \frac{B_z}{B(x)} k_y - \frac{B_y(x)}{B(x)} k_z, \quad (17)$$

$$k_{\parallel}(x) = \frac{B_y(x)}{B(x)} k_y + \frac{B_z}{B(x)} k_z. \quad (18)$$

If there is no magnetic shear [$B_y(x) = 0$], we may take $k_{\perp}(x) = k_y$, $k_{\parallel}(x) = k_z$, and $B(x) = B_z$.

The governing equations now read as

$$i \frac{\partial \tilde{n}}{\partial t} + k_{\perp} V_{\perp} \tilde{n} - \left(\frac{k_{\perp} N}{B} \right)' \tilde{\phi} + N k_{\parallel} \tilde{v}_{\parallel} = 0, \quad (19)$$

$$i \frac{\partial \tilde{v}_{\parallel}}{\partial t} + k_{\perp} V_{\perp} \tilde{v}_{\parallel} = \frac{k_{\parallel}}{s^2} \tilde{\phi}, \quad (20)$$

$$\frac{\partial^2 \tilde{\phi}}{\partial x^2} - k^2 \tilde{\phi} = \tilde{n}, \quad (21)$$

where $'$ denotes the derivative with respect to x and $k = \sqrt{k_y^2 + k_z^2}$. The ambient shear flow is

$$V_{\perp}(x) = \frac{x}{B(x)}, \quad V_{\parallel}(x) = 0 \quad (|x| \leq 1). \quad (22)$$

Because the derivative of $N(x)$ yields delta functions, the perturbed density \tilde{n} must include delta functions, representing the surface wave perturbations; we write

$$\tilde{n}(x, t) = a(t) \delta(x+1) + b(t) \delta(x-1) + f(x, t), \quad (23)$$

where $a(t)$ and $b(t)$ represent the amplitudes of the surface waves and $f(x, t)$ is the continuous part of the density fluctuation. We substitute (21) into (19) to eliminate \tilde{n} and obtain

$$i \frac{\partial}{\partial t} \left(\frac{\partial^2 \tilde{\phi}}{\partial x^2} - k^2 \tilde{\phi} \right) + k_{\perp} V_{\perp} \left(\frac{\partial^2 \tilde{\phi}}{\partial x^2} - k^2 \tilde{\phi} \right) - \left(\frac{k_{\perp} N}{B} \right)' \tilde{\phi} + N k_{\parallel} \tilde{v}_{\parallel} = 0. \quad (24)$$

The assumption (23) implies the continuity of $\tilde{\phi}$ at $x = \pm 1$. Integrating (24) in infinitesimal neighborhoods of $x = \pm 1$ yields

$$i \frac{\partial}{\partial t} \left[\frac{\partial \tilde{\phi}}{\partial x} \right]_{x=\pm 1} + k_{\perp} V_{\perp} \left[\frac{\partial \tilde{\phi}}{\partial x} \right]_{x=\pm 1} - \left(\frac{k_{\perp}}{B} \tilde{\phi} \right) (x = \pm 1) = 0, \quad (25)$$

where the square brackets denote the jump across $x = \pm 1$. Using (21) and (23), we obtain

$$\left[\frac{\partial \tilde{\phi}}{\partial x} \right]_{x=-1} = a(t), \quad \left[\frac{\partial \tilde{\phi}}{\partial x} \right]_{x=1} = b(t), \quad (26)$$

which correspond to the surface charges. The same relations have been derived in previous publications,^{6,8} where the dispersion relation of the surface waves (diocotron modes) has been analyzed with Fourier transforming $i \partial_t$ to $-\omega$. This treatment, however, fails to capture nonexponential (algebraic) behavior of the system that stems from the non-Hermitian property of the problem. In this paper, we solve the initial value problem directly.

Finally, we obtain from (19)–(21),

$$i \frac{\partial f}{\partial t} + \frac{k_{\perp}(x)x}{B(x)} f(x,t) - \left(\frac{k_{\perp}(x)}{B(x)} \right)' \tilde{\phi}(x,t) + k_{\parallel}(x) \tilde{v}_{\parallel}(x,t) = 0, \quad (27)$$

$$i \frac{da}{dt} - \frac{k_{\perp}(-1)}{B(-1)} a(t) - \frac{k_{\perp}(-1)}{B(-1)} \tilde{\phi}(-1,t) = 0, \quad (28)$$

$$i \frac{db}{dt} + \frac{k_{\perp}(1)}{B(1)} b(t) + \frac{k_{\perp}(1)}{B(1)} \tilde{\phi}(1,t) = 0, \quad (29)$$

$$i \frac{\partial \tilde{v}_{\parallel}}{\partial t} + \frac{k_{\perp}(x)x}{B(x)} \tilde{v}_{\parallel}(x,t) = \frac{k_{\parallel}(x)}{s^2} \tilde{\phi}(x,t), \quad (30)$$

$$\tilde{\phi}(x,t) = -\frac{1}{2k} \left(a(t) e^{-k|x+1|} + b(t) e^{-k|x-1|} + \int_{-\infty}^{\infty} e^{-k|x-\xi|} f(\xi,t) d\xi \right). \quad (31)$$

III. KELVIN–HELMHOLTZ (DIOCOTRON) MODE AND PLASMA OSCILLATION

A. Perpendicular modes

In this section, we consider a constant magnetic field and perpendicular modes with assuming

$$k_y \neq 0, \quad k_z = 0, \quad B_y(x) = 0. \quad (32)$$

In this case, (19) and (20) are decoupled, and (19) reduces into a simple Rayleigh equation.⁹ Also, in (27)–(31), we can decouple the parallel motion of electrons represented by (30). Density evolution equations are cast in the matrix form

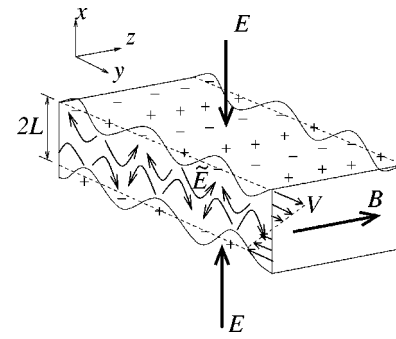


FIG. 1. Diocotron instability in slab electron plasmas.

$$-i \frac{\partial}{\partial t} \begin{pmatrix} f(x) \\ a \\ b \end{pmatrix} = \begin{pmatrix} \frac{k_y}{B} x & 0 & 0 \\ \frac{k_y}{B} \mathcal{G}_{-1} & -\frac{1}{2B} (2k_y - 1) & \frac{1}{2B} e^{-2k_y} \\ -\frac{k_y}{B} \mathcal{G}_1 & -\frac{1}{2B} e^{-2k_y} & \frac{1}{2B} (2k_y - 1) \end{pmatrix} \times \begin{pmatrix} f(x) \\ a \\ b \end{pmatrix}, \quad (33)$$

where

$$\mathcal{G}_x f = \frac{1}{2k} \int_{-\infty}^{\infty} e^{-k|x-\xi|} f(\xi) d\xi. \quad (34)$$

When we take $f(x) = 0$, the coupling of two surface waves $a(t)$ and $b(t)$ determines the eigenvalue

$$\lambda_{\pm} = i\omega_{\pm} = \pm \frac{i}{2B} \sqrt{(2k_y - 1)^2 - e^{-4k_y}}. \quad (35)$$

These frequencies ω_{\pm} are consistent to the well-known diocotron mode dispersion relation in the surface wave model.⁸ The surface waves produce perturbed electrostatic potential $\tilde{\phi}$ through which both waves interact. The dispersion relation is determined by connecting $\tilde{\phi}$ at $x = \pm 1$ [see (28) and (29)], which is expressed by the lower two components of the matrix equation (33). For $k_y < k_c \approx 0.639$, the frequency ω_{\pm} are pure imaginary numbers representing the diocotron instability. The physical mechanism of the diocotron instability is illustrated in Fig. 1. Perturbations on the two surfaces of the plasma, where the density has jumps, couple with each other through the induced electric field $\tilde{\mathbf{E}}$.¹⁴

The coefficient $k_y x/B$ in the matrix operator of (33) yields an essential singularity resulting in a continuous spectrum. This spectrum represents the mixing effect of the flow shear (see Fig. 2). To see the mathematical structure, let us simplify the equation with taking $a = b = 0$ and $f(\pm 1, t) = 0$ to obtain

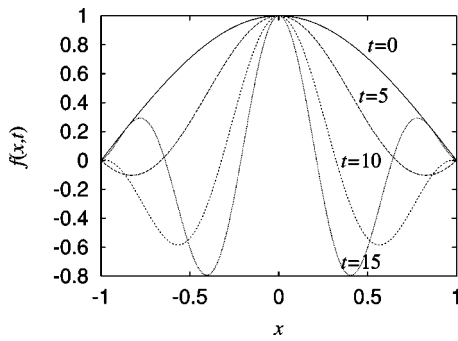


FIG. 2. Mixing of the inner density fluctuation $f(x,t)$.

$$\left(\omega - \frac{k_y x}{B}\right) f = 0. \tag{36}$$

The multiplication of x reads as the ‘‘coordinate operator.’’ Any function of the form $f(x) = e^{i\omega t} \delta(x - x_s)$ is a solution to (36) when $\omega = k_y x_s / B$ with x_s inside the plasma layer, meaning that ω in the range of $-k_y / B < \omega < k_y / B$ is a continuous spectrum. Similarly, (24) has singular eigenfunctions corresponding to the flow shear continuum spanning the range of $\{k_\perp(x) V_\perp(x), -1 < x < 1\}$. If we take $g \equiv (\omega - k_y x / B) f$ as a variable, we overlook the continuous spectrum. However, such treatment is physically irrelevant and mathematically wrong, as already pointed out by Case.¹⁵

Because of the non-Hermitian property of the Rayleigh equation, the frequency spectrum ω does not simply predict the temporal evolution of the system. For the stable case ($k_y > k_c$), we find that the frequencies of the coupled surface waves lie in the range of the continuous spectrum. It is remarkable that resonance (frequency overlapping) of the surface-wave spectrum and the continuous spectrum results in degenerate eigenvalue (nilpotent) reflecting the non-Hermitian property of the system. A delta function placed at the ‘‘resonant surface’’

$$x = \mu_\pm \equiv \pm \frac{1}{2k_y} \sqrt{(2k_y - 1)^2 - e^{-4k_y}} \tag{37}$$

is included in the singular eigenfunction belonging to the continuous spectrum, which has the same frequency with one of the surface waves.

When two regular modes satisfy the resonance condition, the degeneracy of the eigenfunction brings about a new mode (generalized eigenfunction) that grows in proportion to t . However, singular eigenfunctions belonging to the continuous spectrum receive the mixing effect, resulting in saturation of the algebraic growth. Figure 3 demonstrates the transient algebraic growth followed by saturation, which is caused by the presence of off-diagonal terms including \mathcal{G} ; the integral operator \mathcal{G} brings about the phase-mixing damping. Here, we have assumed an initial condition

$$f(x,0) = \exp\left\{-\left(\frac{x - \mu_+}{0.05}\right)^2\right\}, \tag{38}$$

and $k_y = 1.0$, $a(0) = b(0) = 0.0$.

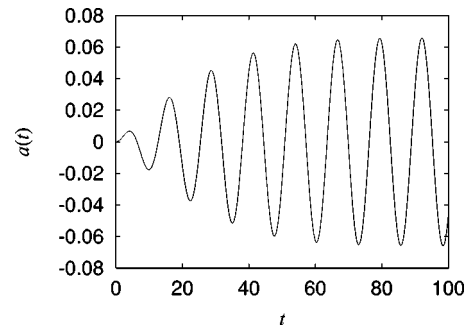


FIG. 3. Time evolution of the surface wave amplitude $a(t)$ for the Gaussian initial profile.

B. Oblique modes (diocotron-plasma oscillation coupling)

Before considering a sheared magnetic field configuration, we study the coupling of the perpendicular and parallel motions in a homogeneous magnetic field with assuming an oblique wave vector $\mathbf{k} = (k_y, k_z)$. In order to incorporate the parallel motion, we set

$$k_y \neq 0, \quad k_z \neq 0, \quad B_y(x) = 0. \tag{39}$$

The parallel wave number k_z yields coupling between (27) and (30), and hence, we must solve the whole set of (27)–(31) simultaneously. Spectral analysis¹⁰ show that exponential instabilities (ω with an imaginary part) are removed for small s^2 . This stabilizing effect is explained by the short circuit of the perturbation charges through the parallel motion of electrons. The electron motion in the direction parallel to the magnetic field is much faster than the diocotron oscillation, if $s^2 \ll 1$. A finite k_z couples the fast electron motion and diocotron oscillation. In addition to the modification of the diocotron and continuous spectra, a new set of discrete spectra appears. They are always discrete real eigenvalues ranged outside of the continuous spectrum.¹⁰

We also observe complex (nonexponential) phenomena reflecting the non-Hermitian property of the system. Interesting secular behavior is well visible in the range of $k_y \gg k_z \sim O(s)$. For an arbitrary initial condition, the local oscillation amplitude increase remarkably near the ‘‘resonant surfaces.’’ Figure 4 shows the result of simulation with $s = 10^{-2}$, $k_y = 1.0$, and $k_z = 10^{-3}$ (the arrows indicate the reso-

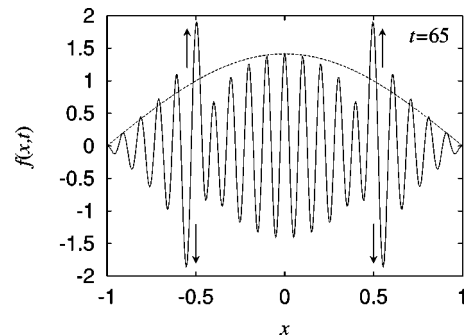


FIG. 4. The density $f(x,t)$ at $t=65$. The initial condition is $f(x,0) = \sqrt{2} \cos(\pi x / 2)$. The amplitude increases near the resonant surfaces $x = \mu_\pm (= \pm 0.495)$.

nant surfaces and the dashed line shows the initial condition). The divergence of the resonant-oscillation amplitude is proportional to t .

The mathematical structure of this secular behavior is illustrated as follows. We rewrite (27)–(31) in a matrix form

$$-i \frac{\partial}{\partial t} \begin{pmatrix} f(x) \\ \tilde{v}_{\parallel}(x) \\ a \\ b \end{pmatrix} = \begin{pmatrix} \frac{k_y}{B}x & k_z & 0 & 0 \\ \frac{k_z}{s^2} \mathcal{G}_x & \frac{k_y}{B}x & \frac{k_z}{2ks^2} e^{-k|x+1|} & \frac{k_z}{2ks^2} e^{-k|x-1|} \\ \frac{k_y}{B} \mathcal{G}_{-1} & 0 & -\frac{k_y}{2kB} (2k-1) & \frac{k_y}{2kB} e^{-2k} \\ -\frac{k_y}{B} \mathcal{G}_1 & 0 & -\frac{k_y}{2kB} e^{-2k} & \frac{k_y}{2kB} (2k-1) \end{pmatrix} \begin{pmatrix} f(x) \\ \tilde{v}_{\parallel}(x) \\ a \\ b \end{pmatrix}, \tag{40}$$

where the operator \mathcal{G}_x is defined by (34). If k_z is small, the mixing effect is dominant and $f(x,t)$ becomes highly oscillatory with respect to x for large t (see Fig. 2). Then, the integral of (34) becomes small (the phase mixing damping). Neglecting the integral term (\mathcal{G}) in (40), we obtain “local” oscillation equations. (In a more exact analysis with retaining the integral term, spatial correlations remain, however, we will leave this problem for future studies.) We rewrite λ_{\pm} , μ_{\pm} more generally as

$$\lambda_{\pm} = i\omega_{\pm} = \pm \frac{ik_y}{2Bk} \sqrt{(2k-1)^2 - e^{-4k}}, \tag{41}$$

$$\mu_{\pm} = \pm \frac{1}{2k} \sqrt{(2k-1)^2 - e^{-4k}}. \tag{42}$$

Observing $f(x)$ at $x = \mu_+$ (or $x = \mu_-$), (40) reads

$$-i \frac{d}{dt} \begin{pmatrix} f(\mu_+) \\ \tilde{v}_{\parallel}(\mu_+) \\ a \\ b \end{pmatrix} = \begin{pmatrix} \frac{k_y}{B} \mu_+ & k_z & 0 & 0 \\ 0 & \frac{k_y}{B} \mu_+ & \frac{k_z}{2ks^2} e^{-k|\mu_++1|} & \frac{k_z}{2ks^2} e^{-k|\mu_+-1|} \\ 0 & 0 & -\frac{k_y}{2kB} (2k-1) & \frac{k_y}{2kB} e^{-2k} \\ 0 & 0 & -\frac{k_y}{2kB} e^{-2k} & \frac{k_y}{2kB} (2k-1) \end{pmatrix} \begin{pmatrix} f(\mu_+) \\ \tilde{v}_{\parallel}(\mu_+) \\ a \\ b \end{pmatrix}. \tag{43}$$

The generator of (43) can be written in a Jordan canonical form

$$\mathbf{T} \begin{pmatrix} \lambda_+ & 1 & 0 & 0 \\ 0 & \lambda_+ & 1 & 0 \\ 0 & 0 & \lambda_+ & 0 \\ 0 & 0 & 0 & \lambda_- \end{pmatrix} \mathbf{T}^{-1}, \tag{44}$$

and a nonorthogonal transform

$$\mathbf{T} = (\psi_1 \quad \psi_2 \quad \psi_3 \quad \psi_4) \tag{45}$$

$$= \begin{pmatrix} -k_z q_+ & 0 & 0 & q_- k_z / 4\omega_-^2 \\ 0 & i q_+ & 0 & q_- / 2\omega_- \\ 0 & 0 & e^{-2k} & e^{-2k} \\ 0 & 0 & p_+ & p_- \end{pmatrix}, \tag{46}$$

where

$$p_{\pm} = (2k-1) \pm \sqrt{(2k-1)^2 - e^{-4k}}, \tag{47}$$

$$q_{\pm} = \frac{k_z}{2ks^2} (e^{-k|\mu_++1|} e^{-2k} + e^{-k|\mu_+-1|} p_{\pm}). \tag{48}$$

Since ψ_2 and ψ_3 are the generalized eigenfunctions representing the nilpotent, the general solution to the evolution equation (43) takes the form

$$\begin{aligned} \psi = & (C_1 + C_2 t + C_3 t^2) e^{\lambda_+ t} \psi_1 + (C_2 + C_3 t) e^{\lambda_+ t} \psi_2 \\ & + C_3 e^{\lambda_+ t} \psi_3 + C_4 e^{\lambda_- t} \psi_4, \end{aligned} \tag{49}$$

where $C_i (i=1, \dots, 4)$ are constants to be determined by the initial condition. For example, if we take

$$C_3 = 1.0, \quad C_1 = C_2 = C_4 = 0.0, \tag{50}$$

the surface waves of a and b show harmonic oscillations with frequency ω_+ , which generate the oscillation of

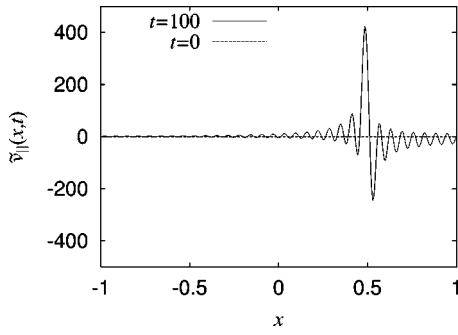


FIG. 5. Profile of parallel electron velocity $\tilde{v}_{\parallel}(x,t)$ at $t=100$. The initial condition is given by (50). Near the resonant surface ($x=\mu_+=0.495$), large oscillation appears.

electrostatic potential $\tilde{\phi}$. This $\tilde{\phi}$ resonates with the parallel electron motion at $x=\mu_+$, and the amplitude of $\tilde{v}_{\parallel}(\mu_+)$ increases in proportion to t . The $\tilde{v}_{\parallel}(\mu_+)$ also resonates with $f(\mu_+)$, resulting in amplification of $f(\mu_+)$ in proportion to t^2 . Indeed, in (27)–(31), $\tilde{\phi}$ and \tilde{v}_{\parallel} act as forcing terms for each oscillation. Formally, the solution is written as

$$a(t) = e^{-2k} e^{i\omega t}, \tag{51}$$

$$\tilde{v}_{\parallel}(\mu_+, t) = iq_+ t e^{i\omega t}, \tag{52}$$

$$f(\mu_+, t) = -k_z q_+ t^2 e^{i\omega t}. \tag{53}$$

In the above discussion, we have assumed a much simplified model where the system is represented by a localized system of four dimensional coupled oscillators. In careful comparison of this estimate with numerical results, however, we find a significant difference at large t . Figures 5–9 show the result of simulation with $s=10^{-2}$, $k_y=1.0$, and $k_z=10^{-3}$. This discrepancy is caused by the integral operators \mathcal{G} in (40), which yield the continuum damping of the surface wave oscillations a and b . The damping due to the operators $\mathcal{G}_{\pm 1}$ is seen to be exponential in time by the numerical simulation (with damping rate $\nu=0.00565$; see Fig. 7). If we include the damping of the surface waves in the expression

$$a(t) = e^{-2k} e^{(i\omega + \nu)t}, \tag{54}$$

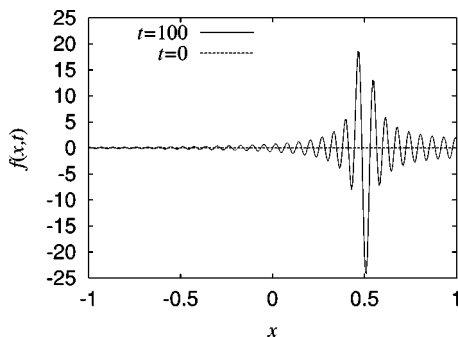


FIG. 6. Profile of density fluctuation $f(x,t)$ at $t=100$. The initial condition is given by (50). Near the resonant surface ($x=\mu_+=0.495$), large oscillation appears.

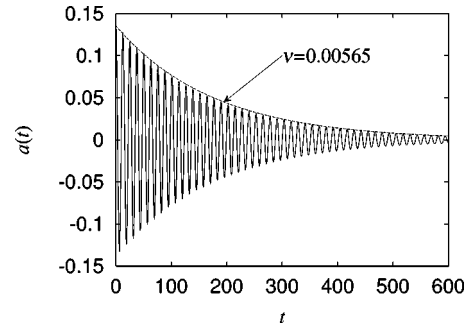


FIG. 7. Time evolution of the surface density fluctuation $a(t)$. The initial condition is given by (50). Dashed line denotes the function $e^{-2k} e^{-\nu t}$. Continuum damping is found to be exponential with $\nu=0.00565$.

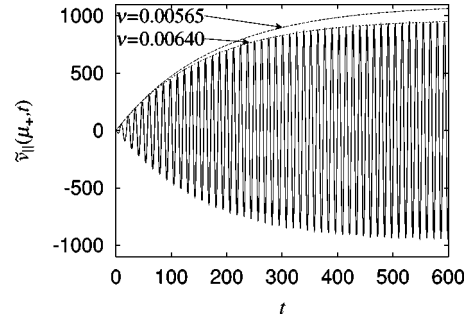


FIG. 8. Time evolution of the parallel electron velocity $\tilde{v}_{\parallel}(x,t)$ at $x=\mu_+$. The initial condition is given by (50). Dashed lines denote the function $q_+(1-e^{-\nu t})/\nu$.

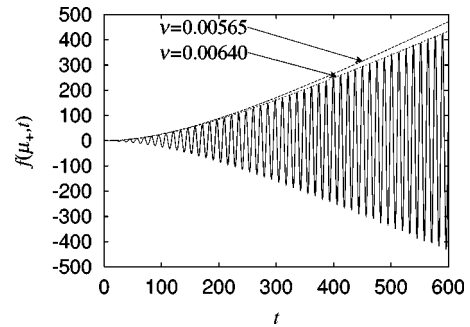


FIG. 9. Time evolution of the inner density fluctuation $f(x,t)$ at $x=\mu_+$. The initial condition is given by (50). The amplitude starts to grow in proportion to t^2 and converges to asymptotic growth $\propto t$. Dashed lines denote the function $(k_z q_+ / \nu) \{ (1-e^{-\nu t}) / \nu - t \}$.

then \tilde{v}_{\parallel} and f are evaluated as

$$\tilde{v}_{\parallel}(\mu_+, t) = iq_+ e^{i\omega t} \frac{1-e^{-\nu t}}{\nu}, \tag{55}$$

$$f(\mu_+, t) = -k_z q_+ e^{i\omega t} \left(t - \frac{1-e^{-\nu t}}{\nu} \right) \frac{1}{\nu}. \tag{56}$$

In Figs. 8 and 9, we compare these solutions with the simulation. The damping coefficient $\nu=0.00565$, evaluated by

the damping of a , is still insufficient, because we have another integral operator, \mathcal{G}_x , in (40). We observe that $\nu = 0.00640$ fits the simulation result.

In summary, the density fluctuation starts to grow at the resonant surface in proportion to t^2 (mode interaction due to non-Hermitian property), while the mixing effect decelerates the growth down to t .

IV. EFFECT OF MAGNETIC SHEAR

In this section, we consider a sheared magnetic field assuming

$$k_y \neq 0, \quad k_z = 0, \quad B_y(x) = \alpha x, \tag{57}$$

where α is a given constant representing the strength of magnetic shear.

First, we solve the eigenvalue problem numerically. In Fig. 10, we show the stable (real ω) and unstable region (gray), in the k_y - α space. In the unstable region (gray), ω is a pure imaginary number and the growth rate is a strong function of the magnetic shear parameter α (Fig. 11). The instability is related to a “rational surface” where \mathbf{k} is perpendicular to the ambient magnetic field. Electric charges at the rational surface ($k_{\parallel} = 0$) are not short-circuited, and produce unstable modes (Fig. 12).

In order to explain band structure of unstable modes, we replace $-i\partial/\partial t$ by ω in (27)–(31), and eliminate a, b, f , and \tilde{v}_{\parallel} to obtain

$$\begin{aligned} \tilde{\phi}''(x) + \left\{ -k^2 + \frac{1}{\omega - k_{\perp}(x)V_{\perp}(x)} \left(\frac{k_{\perp}(x)}{B(x)} \right)' \right. \\ \left. + \frac{k_{\parallel}^2(x)}{s^2(\omega - k_{\perp}(x)V_{\perp}(x))^2} \right\} \tilde{\phi}(x) = 0 \quad (-1 < x < 1). \end{aligned} \tag{58}$$

The boundary conditions are

$$\begin{aligned} \tilde{\phi}'(-1) + \left(\frac{k_{\perp}(-1)}{(\omega - k_{\perp}(-1)V_{\perp}(-1))B(-1)} - k \right) \\ \times \tilde{\phi}(-1) = 0 \quad (x = -1), \end{aligned} \tag{59}$$

$$\tilde{\phi}'(1) + \left(\frac{k_{\perp}(1)}{(\omega - k_{\perp}(1)V_{\perp}(1))B(1)} + k \right) \tilde{\phi}(1) = 0 \quad (x = 1). \tag{60}$$

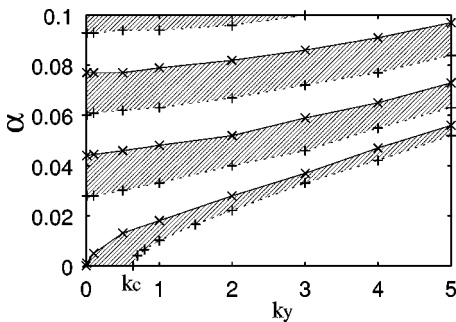


FIG. 10. Unstable region (gray) in k_y - α space.

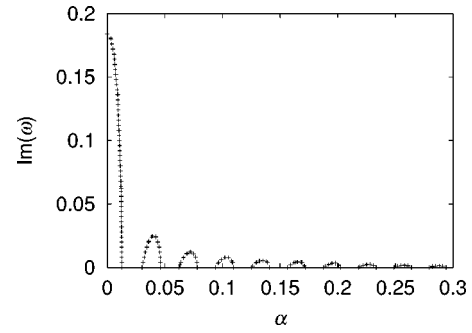


FIG. 11. Growth rate as a function of the magnetic shear parameter α ($k_y = 0.5$).

The marginal stability is found by setting $\omega = 0$. For $B_z = 1$, $B_y(x) = \alpha x$, $k_z = 0$, and $\omega = 0$, (58)–(60) reduce into

$$\frac{d^2 \tilde{\phi}}{dx^2} + \left\{ -k_y^2 + \frac{2\alpha^2}{1 + \alpha^2 x^2} + \frac{\alpha^2}{s^2} (1 + \alpha^2 x^2) \right\} \tilde{\phi} = 0, \tag{61}$$

$$\tilde{\phi}'(-1) + (1 - k) \tilde{\phi}(-1) = 0, \tag{62}$$

$$\tilde{\phi}'(1) - (1 - k) \tilde{\phi}(1) = 0. \tag{63}$$

We solve these equations as an eigenvalue problem with respect to α , and obtain discrete eigenvalues $\{\alpha_i\}$. Changing the parameter k_y , we can draw the marginal stability curve in the k_y - α space (Fig. 10). The potential of (61),

$$G(x, \alpha) \equiv -k_y^2 + \frac{2\alpha^2}{1 + \alpha^2 x^2} + \frac{\alpha^2}{s^2} (1 + \alpha^2 x^2), \tag{64}$$

satisfies

$$\lim_{\alpha \rightarrow +\infty} G(x, \alpha) = +\infty \quad (\forall x). \tag{65}$$

Applying Sturm’s oscillation theorems,¹⁶ we find that the accumulation point of $\{\alpha_i\}$ is infinity, implying that, in any large α regime, the unstable region appears. If there is no rational surface, G would be a singular function, and Sturm’s theorem does not apply.

Next, we study how the secular behavior is modified by the effect of magnetic shear. Equations (27)–(31) are now written as

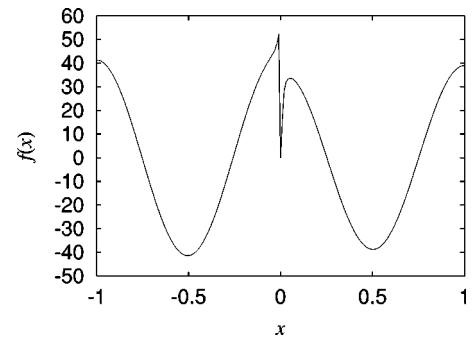


FIG. 12. Unstable eigenfunction in a magnetic shear configuration with $B_y(x) = \alpha x$. Rational surface is $x = 0$.

$$-i \frac{\partial}{\partial t} \begin{pmatrix} f(x) \\ \tilde{v}_{\parallel}(x) \\ a \\ b \end{pmatrix} = \begin{pmatrix} \frac{k_{\perp}(x)}{B(x)} x + F(x) \mathcal{G}_x & k_{\parallel}(x) & \frac{F(x)}{2k} e^{-k|x+1|} & \frac{F(x)}{2k} e^{-k|x-1|} \\ \frac{k_{\parallel}(x)}{s^2} \mathcal{G}_x & \frac{k_{\perp}(x)}{B(x)} x & \frac{k_{\parallel}(x)}{2ks^2} e^{-k|x+1|} & \frac{k_{\parallel}(x)}{2ks^2} e^{-k|x-1|} \\ \frac{k_{\perp}(-1)}{B(-1)} \mathcal{G}_{-1} & 0 & -\frac{k_{\perp}(-1)}{2kB(-1)} (2k-1) & \frac{k_{\perp}(-1)}{2kB(-1)} e^{-2k} \\ -\frac{k_{\perp}(1)}{B(1)} \mathcal{G}_1 & 0 & -\frac{k_{\perp}(1)}{2kB(1)} e^{-2k} & \frac{k_{\perp}(1)}{2kB(1)} (2k-1) \end{pmatrix} \begin{pmatrix} f(x) \\ \tilde{v}_{\parallel}(x) \\ a \\ b \end{pmatrix}, \quad (66)$$

where

$$F(x) = \frac{d}{dx} \left(\frac{k_{\perp}(x)}{B(x)} \right). \quad (67)$$

Equation (66) is more complicated than (40), since k_{\perp} , k_{\parallel} , and B depend on x , and, moreover, new terms including F are added. For $k_y \gg \alpha \sim O(s)$, neglecting the terms including the integral operator \mathcal{G} , we can derive a Jordan canonical form similar to (44). Numerical solution of the initial value problem shows the same secular behavior as Figs. 7–9 in the region of real ω . Since the oscillations of a and b are damped, the effect of F disappears rapidly, and the asymptotic behavior is unchanged.

V. SUMMARY

We have studied the electrostatic Kelvin–Helmholtz (diocotron) instabilities in a sheared magnetic field. Because of the non-Hermitian property of the system, the coupling of the Kelvin–Helmholtz modes and the parallel plasma oscillation produces rather complex phenomena.

Interesting transient behavior has been found in oblique modes. The generator of the system contains two degenerate continuous spectra ($\omega - kV = 0$), one originates from the density evolution equation and the other from parallel equation of motion. The nonorthogonality of the corresponding eigenfunctions (reflecting the non-Hermitian property of the system) yields a coupling of the two branches of spectra. This “resonance” brings about a spatially localized and temporally algebraic ($\propto t$) density fluctuation. In the exponent of this secularity, we observe a signature of the essential singularity of the continuous spectra.

The growth of the parallel velocity at the resonant surface saturates after a short time. This is due to the phase mixing induced by the integral operator \mathcal{G} appearing in the off-diagonal part of the generator [see (40)]. If one assumed a prompt damping of the continuous density perturbation

$f(x)$ and neglected the integral terms (including \mathcal{G}), the surface waves will approach constant amplitude oscillations and the localized mode will grow in proportion to t^2 . However, the damping of $f(x)$ is rather slow and its persistence yields a long term coupling with the surface waves, resulting in the damping of the surface waves. Including appropriate asymptotic forms for the integral terms, we can reconstruct the exact exponent of the secularity.

In a magnetic shear configuration, rational surfaces ($k_{\perp} = 0$) exist inside the plasmas, where the parallel short-circuit effect does not work, resulting in unstable (complex ω) modes. Further calculations for smooth equilibrium densities will be reported elsewhere.

ACKNOWLEDGMENTS

This work is partially supported by a Grant-in-Aid from the Japanese Ministry of Education, Culture, Sports, Science and Technology, No. 09308011 and No. 12780353.

¹Z. Yoshida, Y. Ogawa, J. Morikawa *et al.*, *Non-Neutral Plasmas Physics III*, AIP Conference Proceedings 498 (AIP, New York, 1999), p. 397.

²S. Robertson and B. Walch, *Phys. Plasmas* **7**, 2340 (2000).

³K. Avinash, *Phys. Plasmas* **1**, 3731 (1994).

⁴R. C. Davidson, K. T. Tsang, and J. A. Swegle, *Phys. Fluids* **27**, 2332 (1984).

⁵S. Riyopoulos, *Phys. Plasmas* **6**, 323 (1999).

⁶R. C. Davidson, *Physics of Nonneutral Plasmas* (Addison-Wesley, Redwood, 1990).

⁷S. Chandrasekhar, *Hydrodynamic and Hydromagnetic Stability* (Dover, New York, 1961).

⁸A. Hasegawa, *Plasma Instabilities and Nonlinear Effects* (Springer-Verlag, Berlin, 1975), p. 129.

⁹C. F. Driscoll and K. S. Fine, *Phys. Fluids B* **2**, 1359 (1990).

¹⁰S. Kondoh, T. Tatsumo, and Z. Yoshida, *Phys. Plasmas* **8**, 2635 (2001).

¹¹F. Volponi, Z. Yoshida, and T. Tatsumo, *Phys. Plasmas* **7**, 2314 (2000).

¹²T. Tatsumo, F. Volponi, and Z. Yoshida, *Phys. Plasmas* **8**, 399 (2001).

¹³R. A. Smith and M. N. Rosenbluth, *Phys. Rev. Lett.* **64**, 649 (1990).

¹⁴W. Knauer, *J. Appl. Phys.* **37**, 602 (1966).

¹⁵K. M. Case, *Phys. Fluids* **3**, 143 (1960).

¹⁶E. L. Ince, *Ordinary Differential Equations* (Dover, New York, 1926).